RSC Advances

ROYAL SOCIETY OF CHEMISTRY

www.rsc.org/advances

Journal Name

RSCPublishing

COMMUNICATION

Bio-templated fabrication of hierarchically porous WO_3 microspheres from lotus pollens for NO gas sensing at low temperatures

Cite this: DOI: 10.1039/x0xx00000x

Received 00th January 2012,
Accepted 00th January 2012

DOI: 10.1039/x0xx00000x

www.rsc.org/

Xiao-Xue Wang,[a#] Kuan Tian,[a#] Hua-Yao Li,[a] Ze-Xing Cai[a] and Xin Guo[a]*

Lotus pollens were used as templates to prepare WO_3 microspheres; the intriguing structural features of the pollens, e.g. hollow sphere with highly porous double shells, were perfectly inherited by the WO_3 microspheres. The hierarchically porous structure of the WO_3 microspheres was ideal for gas sensing. The WO_3 microsphere-based sensor exhibited a high sensitivity (S = 46.2) to 100 ppm NO gas with a pretty fast response and recovery speed (62 s/223 s) at 200 °C. Compared with NO sensors reported in literatures so far, the WO_3 microsphere-based sensor has among the highest sensitivity and fastest response/recovery.

Accurate early detection of nitric oxide (NO) under low concentrations at low temperatures is important for many reasons. First of all, NO is a hazardous gas; its threshold limit value (TLV), i.e. the maximum concentration allowable for repeated exposure without producing adverse health effects, is only 25 ppm.[1] On the other hand, inhaled nitric oxide (INO) therapy is widely applied in the heart valve surgery of adults, the INO delivery and monitoring system requires that the NO concentration must be controlled below 40 ppm.[2]Current state-of-the-art NO gas sensors are mostly operated at temperatures above 200ºC;[3]the high operation temperature causes high power consumption and potential safety hazards.

Tungsten trioxide (WO_3), an n-type semiconductor with a bandgap of 2.8 eV, is a very promising sensing material owing to its excellent sensitivity to NO.[4] Material morphology plays an important role in the gas sensing properties.[5-7] Hence, various morphologies with different dimensional structures have been synthesized to improve the performance of devices based on WO_3.[8] Yin et al.[9] reported that WO_3 nanoplates performed high sensitivity and selectivity to NO. Zhang et al.[10] reported that TiO_2(B) nanoparticle-functionalized WO_3 nanorods showed great sensitivity at low temperatures (150 ~ 350 ºC). Shim et al.[11] synthesized the Au-decorated WO_3 cross-linked nanodomes, and found that the sensor exhibited extremely high sensitivities and selectivities, and ppt-level detection limits to NO_2 and C_2H_5OH. Yan et al.[12] prepared nanobrick clusters-based sensor, and achieved high sensitivity towards NO_2. Yin et al.[13] improved the H_2S sensing performance by fabricating hierarchical Fe_2O_3@WO_3 nanostructures. Choi et al.[14] reported that an Rh-loaded WO_3 hollow sphere chemiresistive sensor can achieve fast acetone response and low detection limit.

Recently, the bio-templating technique has become a versatile route to fabricate advanced materials with controlled nano/microstructures and desired functions.[15] There are various fantastic bio-templates in our nature, such as cotton fibers,[16] cellulose,[17] butterfly wings,[18] rape pollen grain[19] and lotus pollens[15], etc. Above all, lotus pollens, with hierarchically porous structures, are attracting significant attention owing to its high surface areas, large pore volumes. These unique morphologies and microstructures make them promising candidates for a variety of applications such as bioseparation, catalysis, pollution control, chemical sensing and biomedicine.[19]

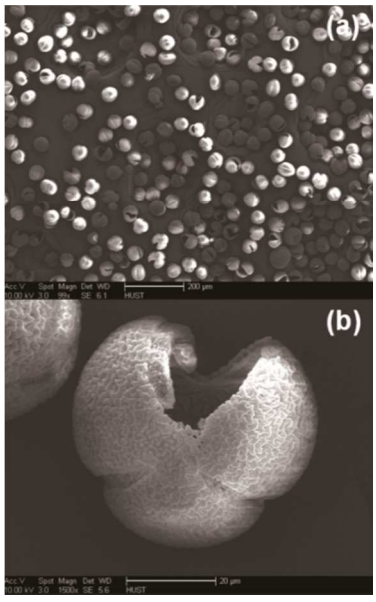

Fig. 1 SEM images of pollen templates.

In this work, hierarchically porous WO_3 microspheres were successfully synthesized via a facile bio-templating method using lotus pollens as the template. Owing to its unique morphology, the WO_3 microsphere-based sensor exhibited a high sensitivity and fast response/recovery towards NO gas at low temperatures.

Pollen templates were prepared by a three-step process. Firstly, purchased pollens were cleaned by immersing, for example, 0.5 g pollen grains into 50 mL ethanol with ultrasonic treatment for 1 h. Then the pollen morphology was fixed by immersing the cleaned pollen grains in the mixed solution of formaldehyde and ethanol (1:1 in volume) for 10 min. Afterwards, the fixed pollen grains were dehydrated by adding the pollens into, for example, 50 mL 12 M sulphuric acid solution and stirred at 80 °C for 4 h. After each step, the pollen grains were filtered and washed with ethanol and deionized water several times. The final product was dried at 80 °C for 12 h. The scanning electron microscopy (SEM, Sirion 200) image of the pollen templates is shown in Fig. 1; the templates are hollow and hierarchically porous microspheres. According to the X-ray powder diffraction (XRD, Philips diffractometer /PW3050 X, Cu-Kα radiation) pattern given in Fig. 2 (a), the templates are amorphous.

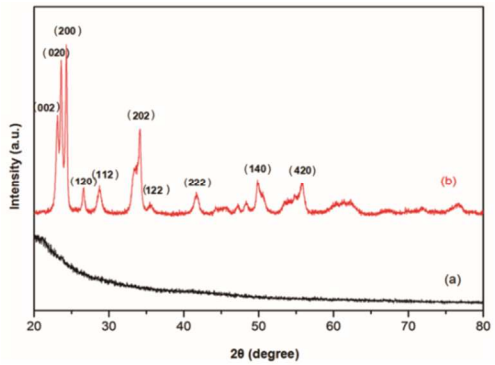

Fig. 2 XRD patterns of (a) pollen templates and (b) WO_3 microspheres.

WO_3 sol was prepared according to the following procedure. 3 g of tungsten acid was added into a 25 mL of solution, which was prepared by mixing 15 mL of 30% hydrogen peroxide solution and 10 mL of ethanol with 30 min ultrasonic treatment. 5 mL of 2M citric acid solution was added into the above suspension drop by drop. Afterwards, 3M aqueous ammonium was added to adjust the pH value to ~4. The resulted mixture was refluxed at 80°C for 30 min under constant stirring until a homogeneous clear sol was obtained.

The spin-coating technique was used to fabricate gas sensors from the WO_3sol. A piece of FTO glass (Nippon Sheet Glass, Japan), on which a gap of about 60 mm was cut by laser, was ultrasonically cleaned with ethanol and distilled water for 10 min. 0.3 g of the pollen templates were dispersed in the WO_3 sol prepared in the above under continuous magnetic stirring. Then the suspension was dripped on the FTO substrate, which was spun at 5000 rpm for 30 *s*. Afterwards, the WO_3 sol on the FTO glass substrate was calcined at 400 ºC for 2 h. According to the XRD pattern given in Fig. 2 (b), WO_3 assumed a monoclinic structure after calcination, and no second phase was detected.

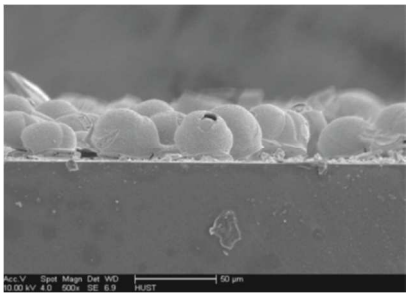

Fig. 3 SEM image of the cross-section of gas sensor based on WO_3 microspheres.

The cross-section of the WO_3 sensor fabricated by spin-coating is shown in Fig. 3. From Fig. 3 one can see that a single layer of WO_3 microspheres were coated on the FTO surface and the layer thickness is circa 25 μm. The microstructure of the WO_3 microspheres is more clearly presented in Fig. 4. From Figs. 4 (a) and (b), one can clearly see that the porous spherical structure of the templates was perfectly inherited by the WO_3 microspheres, and the diameter of the microspheres is mostly in the range of 20 to 30 μm. Furthermore, the shell of each WO_3 microsphere consists of two ~80 nm thick layers, and both the outer and inner layers are highly porous (Figs. 4 (b) to (d)). The intriguing 3-dimensional hierarchically porous and hollow structure of the WO_3 microspheres is ideal for gas sensing.

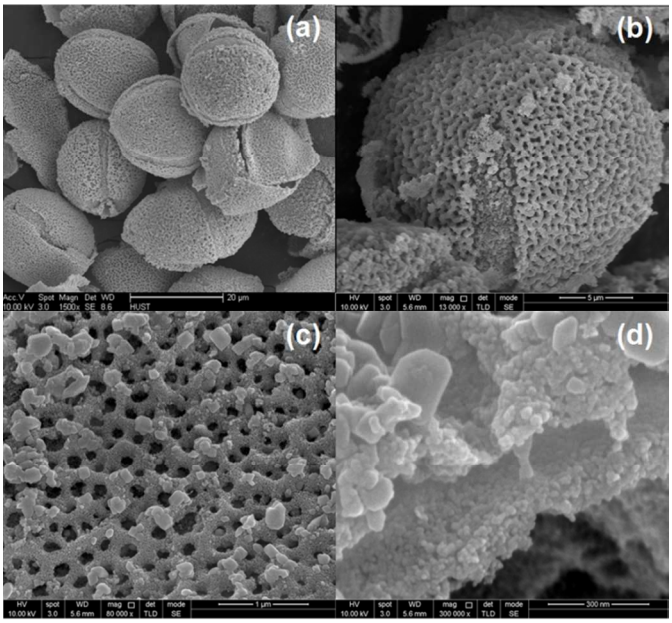

Fig. 4 SEM images of WO_3 microspheres: (a) Low-magnification SEM image, (b) High-magnification SEM image showing the outer surface, (c) the inner surface, (d) the cross-section.

To clearly reveal the hierarchically porous structure of the WO_3 microspheres, transmission electron microscopy (TEM, JEOL 2100F) investigation was also conducted. Fig. 5 (a) shows a typical low-magnification TEM image taken from the shell of a WO_3 microsphere. There is a large quantity of pores with an average diametre under 100 nm, and the number of pores is circa 23 μm^{-2}. Fig. 5 (b) shows a high resolution TEM (HRTEM) image, the shell consists of numerous nanoparticles, and each nanoparticle, the

average diameter of which is ~40 nm, is single crystalline; in a nanoparticle the spacing between two adjacent lattice fringes is 0.3875 nm, and the facet direction is (002), corresponding well to the results of XRD. The hierarchically porous structure remarkably raises the surface active sites and provides nano-aisles to promote sensing properties.

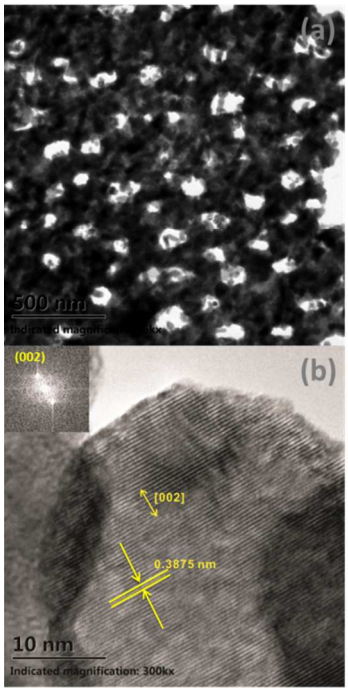

Fig. 5 (a) TEM and (b) HRTEM images of the shell of WO_3 microspheres.

The sensor resistance was measured by the two-probe method, and the data were collected automatically every second using an Agilent B2901A Source Measurement Unit (SMU). In a gas distributing system, NO was mixed with the carrier gas (N_2) to obtain the desired NO concentrations, and introduced into the sample chamber at a flow rate of 100 standard-state cubic centimetre per minute (SCCM). The NO concentration was monitored by an Agilent 7890A Gas Chromatography System. A thermocouple was placed close to the sample surface to accurately monitor the sensor's temperature.

The hierarchically porous WO_3 microspheres-based sensor was very sensitive to NO gas at low temperatures. From the response-recovery curve of the sensor to 100 ppm NO at 200 °C given in Fig. 6 (a), a response (defined as $S = R_{NO} / R_{N_2}$, where R_{NO} and R_{N_2} are the electrical resistances in NO and N_2, respectively) of 46.2 can be determined. And from this figure, the response time t_{resp} and recovery time t_{reco} at 200 °C can also be determined to be 62 and 223 *s* for 90% of full response and recovery, respectively. Despite of the low operation temperature of 200 °C, the response and recovery were pretty fast. Fig. 6 (b) shows the sensor resistance variation under alternating cycles of 50 ppm NO and N_2 at 150 °C. A response of 61.0 was achieved with the response t_{resp} and recovery t_{reco} times being 97 and 2141 *s*, respectively. Even at 150 °C the performance of the WO_3 microsphere-based sensor was reasonably good. Furthermore, good repeatability was achieved among individual alternating cycles at both 200 and 150 °C. The response as a function of temperature under 50 ppm NO is given in Fig. 6 (c). Even at 100 °C, the response is >50, the maximum response was obtained at 150°C, and the response decreases with increasing temperature. Although the response was higher at low temperatures, the recovery time was much long. As a compromise between sensitivity and speed, the optimal working temperature of the porous WO_3 microsphere-based sensor was taken to be 200 °C. The sensing properties to NO gas of the WO_3 microsphere-based sensor are compared with literature results in Table 1; at 200 °C the porous WO_3 microsphere-based sensor has among the highest sensitivity and the rapidest response to the NO sensing. Xie et al.[20] reported that the band gap of C-doped WO_3 microtubes is reduced to 2.12 eV and the introduction of a new intragap band decrease the high-energy requirement for the excitation of electrons from the valence to the conduction band. Therefore, the carbon decomposed from pollens was very favorable for the sensing performance. By doping WO_3 with Cr,[18, 21, 22] or decorating with Pt,[21, 22] Ag[23] or Au[24], the sensing properties can be further improved.

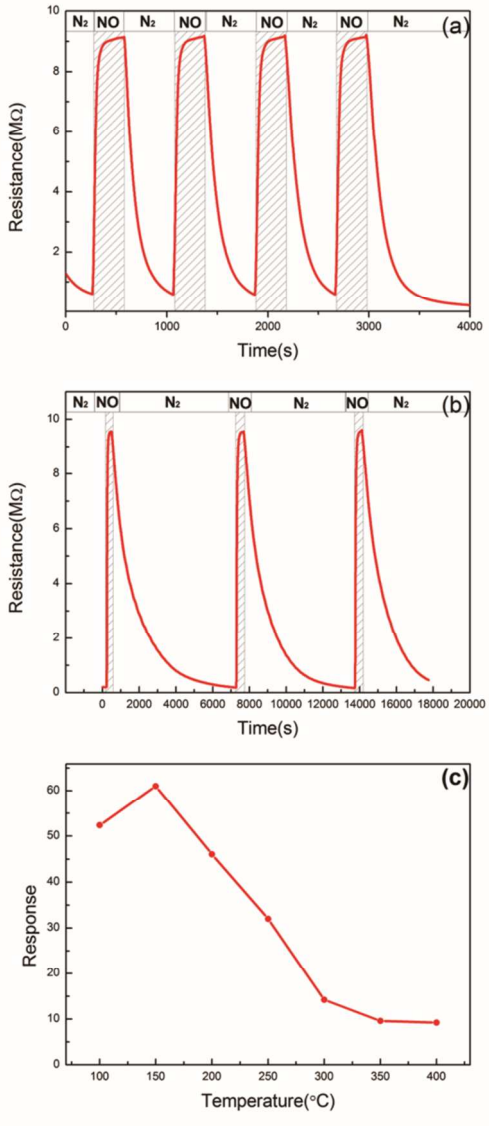

Fig. 6 Response-recovery curve of WO_3microspheres to NO gas: (a) 100 ppm at 200°C, (b) 50 ppm at 150°C, and (c) sensor response to 50 ppm NO at different temperatures.

When exposed to NO, NO molecules are chemisorbed on the surface active sites and take electrons away from the conduction band of WO_3. The reaction is: [31]

$$NO_{(gas)} + e^- + O_{2(ads)} \rightarrow NO_3^-{}_{(ads)} \quad (1)$$

This reaction consumes electrons, therefore, the resistance of WO_3, an *n*-type semiconductor, increases when exposed to NO, as demonstrated by Fig. 6. In the intriguing 3-dimensional hierarchically porous and hollow structure of the WO_3 microspheres, there are innumerable nano-aisles between the outer and inner walls of the microspheres; these nano-aisles are fast pathways for NO and O_2 to travel through the WO_3 shells. It is also worthy of noting that the hierarchically porous structure increases surface area as well as the number of surface active sites. All these structural features of the WO_3 microspheres contribute to the excellent sensing property at low temperatures.

Table 1 Comparison of the sensing properties of various NO sensors.

Material	NO (ppm)	T (°C)	Response	t_{Resp}/t_{Reco} (s)	Ref.
WO_3 powder	5	200	3	600/300	25
Bi_2O_3 thick film	200	360	2.5	--	26
WO_3 thin film	440	250	40	168/270	27
MoO_3 thick film	250	200	80	600/120	28
WO_3 nanopowder	100	250	15	300/1800	29
ZnO urchin-like	0.2	200	12	200/1200	30
WO_3 microspheres	100	200	46	62/223	This work

Conclusions

By means of a pollen-templating method, WO_3 microspheres with all the structural features of lotus pollens were prepared. The WO_3 microspheres had an intriguing 3-dimensional hierarchically porous and hollow structure, which is ideal for gas sensing. The WO_3 microsphere-based sensor exhibited a high sensitivity (response in the range of 31.8 to 61.0) in the temperature range of 100 to 250 °C. The sensitivity decreases with increasing temperature, but at low temperatures, the sensor suffered a slow recovery. As a compromise between sensitivity and speed, the optimal working temperature of the WO_3 microsphere-based sensor was 200 °C. Compared with NO sensors reported in literatures so far, the WO_3 microsphere-based sensor has among the highest sensitivity and fastest response/recovery at 200 °C.

Notes and references

[a] *Laboratory of Solid State Ionics, School of Materials Science and Engineering, Huazhong University of Science and Technology, Wuhan 430074, P. R. China*
**E-mail: xguo@hust.edu.cn*

[#] *These authors contributed equally to this study.*

1 L. Chen, *Sens. Actuator B-Chem.*, 2003, **89**, 68-75.
2 F. Santini, G. Casali, G. Franchi, S. Auriemma, M. Lusini, L. Barozzi, A. Favaro, A. Messina and A. Mazzucco, *Int. J Cardiol.*, 2005, **103**, 156-163.
3 H. Liu, S. Xu, M. Li, G. Shao, H. Song, W. Zhang, W. Wei, M. He, L. Gao, H. Song and J. Tang, *Appl. Phys. Lett.*, 2014, **105**, 163104.
4 J. Huang, Y. Kang, T. Yang, Y. Wang and S. Wang, *J Nat. Gas Chem.*, 2011, **20**, 403-407.
5 C. Zhao, B. Huang, J. Zhou and E. Xie, *Phys. Chem. Chem. Phys.*, 2014, 19327-19332.
6 W. Zhang, Z. Chen and Z. Yang, *Phys. Chem. Chem. Phys.*, 2009, 6263-6268.
7 S. Zhang, F. Ren, W. Wu, J. Zhou, X. Xiao, L. Sun, Y. Liu and C. Jiang, *Phys. Chem. Chem. Phys.*, 2013, 8228-8236.
8 C. Wang, R. Sun, X. Li, Y. Sun, P. Sun, F. Liu and G. Lu, *Sens. Actuator B-Chem.*, 2014, **204**, 224-230.
9 L. Yin, D. Chen, B. Fan, H. Lu, H. Wang, H. Xu, D. Yang, G. Shao and R. Zhang, *Mater. Chem. Phys.*, 2013, **143**, 461-469.
10 H. Zhang, S. Wang, Y. Wang, J. Yang, X. Gao and L. Wang, *Phys. Chem. Chem. Phys.*, 2014, **16**, 10830.
11. Y. S. Shim, H. G. Moon, D. H. Kim, L. Zhang, S. J. Yoon, Y. S. Yoon, C. Y. Kang and H. W. Jang, *RSC Adv.*, 2013, **3**, 10452-10459.
12 A. H. Yan, C. S. Xie, F. Huang, H. Y. Li and S. L. Zhang, *Adv. Mater. Res.*, 2013, **634-638**, 3866-3869.
13 L. Yin, D. Chen, M. Feng, L. Ge, D. Yang, Z. Song, B. Fan, R. Zhang and G. Shao, *RSC Adv.*, 2015, **1**, 328-337.
14 K. I. Choi, S. J. Hwang, Z. Dai, Y. C. Kang and J. H. Lee, *RSC Adv.*, 2014, **4**, 53130-53136.
15 Y. Xia, W. Zhang, Z. Xiao, H. Huang, H. Zeng, X. Chen, F. Chen, Y. Gan and X. Tao, *J Mater. Chem.*, 2012, **22**, 9209.
16 T. Zhang, Y. Zhou, X. Bu, Y. Wang, M. Zhang and J. Hu, *Ceram. Int.*, 2014, **40**, 13703-13707.
17 T. R. Chen, Y. Wang, Y. Wang and Y. Xu, *RSC Adv.*, 2015, **5**, 1673-1679.
18 Z. W. Han, S. C. Niu, W. Li and L. Q. Ren, *Appl. Phys. Lett.*, 2013, **102**, 233702.
19 T. Zhang, Y. Zhou, Y. Wang, X. Bu, H. Wang and M. Zhang, *Appl. Clay Sci.*, 2015, **103**, 67-70.
20 X. H. Ding, D. W. Zeng, S. P. Zhang and C. S. Xie, *Sens. Actuator B-Chem.*, 2011, **155**, 86-92.
21 M. D. Arienzo, M. Crippa, P. Gentile, C. M. Mari, S. Polizzi, R. Ruffo, R. Scotti, L. Wahba and F. Morazzoni, *J Sol-Gel Sci Techn*, 2011, **60**, 378-387.

22 M. D'Arienzo, L. Armelao, C. M. Mari, S. Polizzi, R. Ruffo, R. Scotti and F. Morazzoni, *J Am. Chem. Soc.*, 2011, **133**, 5296-5304.
23 D. Chen, L. Yin, L. Ge, B. Fan, R. Zhang, J. Sun and G. Shao, *Sens. Actuator B-Chem.*, 2013, **185**, 445-455.
24 Q. Xiang, G. F. Meng, H. B. Zhao, Y. Zhang, H. Li, W. J. Ma and J. Q. Xu, *J Phys. Chem. C*, 2010, **114**, 2049-2055.
25 T. Akamatsu, T. Itoh, N. Izu and W. Shin, *Sensors*, 2013, **13**, 12467-12481.
26 A. Cabot, A. Marsal, J. Arbiol and J. R. Morante, *Sens. Actuator B-Chem.*, 2004, **99**, 74-89.
27 M. Penza, C. Martucci and G. Cassano, *Sens. Actuator B-Chem.*, 1998, **50**, 52-59.
28 S. Barazzouk, R. P. Tandon and S. Hotchandani, *Sens. Actuator B-Chem.*, 2006, **119**, 691-694.
29 T. Siciliano, A. Tepore, G. Micocci, A. Serra, D. Manno and E. Filippo, *Sens. Actuator B-Chem.*, 2008, **133**, 321-326.
30 H. N. Hieu, N. M. Vuong, H. Jung, D. M. Jang, D. Kim, H. Kim and S. Hong, *J Mater. Chem.*, 2011, **22**, 1127.
31 M.J. Madou, S.R. Morrison, *Chemical Sensing with Solid State Devices*, Academic Press, San Diego, 1989.